ACCURATE FAST MULTIPOLE SCHEME FOR THE BOUNDARY ELEMENT ANALYSIS OF THREE-DIMENSIONAL LINEAR POTENTIAL PROBLEMS

NEY AUGUSTO DUMONT & HILTON MARQUES SOUZA SANTANA
Department of Civil and Environmental Engineering, Pontifical Catholic University of Rio de Janeiro, Brazil

ABSTRACT

This paper is part of a research work to implement, test, and apply a novel numerical tool that can simulate on a personal computer and in just a few minutes a problem of potential or elasticity with up to tens of millions of degrees of freedom. The first author's group has already developed their own version of the fast multipole method (FMM) for two-dimensional problems, which relies on a consistent construction of the single-layer potential matrix of the collocation boundary element method so that ultimately only polynomial terms (as for the double-layer potential matrix) are required to be integrated along generally curved segments related to a given field expansion pole. The core of the present paper is the mathematical assessment of the double expansions needed in the 3D FMM. The 3D implementation is combined with a particular formulation for linear triangle elements in which all integrations for adjacent source point and boundary element are carried out analytically. As a result, numerical approximations are due exclusively to the FMM series truncations. This allows isolating and testing truncation errors incurred in the series expansions and thus for the first time properly assessing the mathematical features of the FMM, as illustrated by means of two examples. Adaptive numerical quadratures as well as the complete solution of a mixed boundary problem using a GMRES solver, for instance, are just additional tasks and, although already implemented, are not reported herein.
Keywords: boundary elements, fast multipole, machine-precision integration, potential problems, three-dimensional problems.

1 INTRODUCTION

The FMM [1]–[4] is a powerful tool for dealing with very large computational mechanics problems. Our team has already developed a consistent algorithm for general 2D problems [5], [6] with machine-precision integration schemes. We are now working on 3D problems [7], [8] with the combination of analytical evaluations for flat boundary elements, in the case of small source point to element distances [9], [10], and a very convenient adaptive quadrature scheme for intermediary distances [8], [11], [12], that seems to keep being ignored in the technical literature. This paper lays out some conceptual aspects that should make the FMM more consistent and understandable mathematically: we are driven by simplicity. Although the implementation issues of the complete boundary element formulation are not shown, basic accuracy assessments by means of two rather academic examples shall shed light on the practical application possibilities opened up in the present framework.

2 PROBLEM FORMULATION

We are looking for the expansion of the fundamental solution – for three-dimensional problems – about a pole $\mathbf{x}_c$ that is at the distance $r = |\mathbf{x}|$ from the source point $\mathbf{x}_s$, that is, $\mathbf{x} = \mathbf{x}_s - \mathbf{x}_c$ in the classical literature notation, and to be evaluated at a field point $\mathbf{x}_f$ at a distance $\rho = |\mathbf{y}|$ to the expansion pole, that is, $\mathbf{y} = \mathbf{x}_f - \mathbf{x}_c$ (see the left drawing in Fig. 1, which gives the vector orientations we are following in the developments):

$$u^*(\mathbf{x}_f - \mathbf{x}_s) \equiv \frac{1}{4\pi\,|\mathbf{x}_f - \mathbf{x}_s|} = \frac{1}{4\pi} \sum_{n=0}^{N} \sum_{m=-n}^{n} \bar{S}_{n,m}(\mathbf{x}) R_{n,m}(\mathbf{y}) + O\left((\rho/r)^{N+1}\right), \quad (1)$$

WIT Transactions on Engineering Sciences, Vol 134, © 2022 WIT Press
www.witpress.com, ISSN 1743-3533 (on-line)
doi:10.2495/BE450011

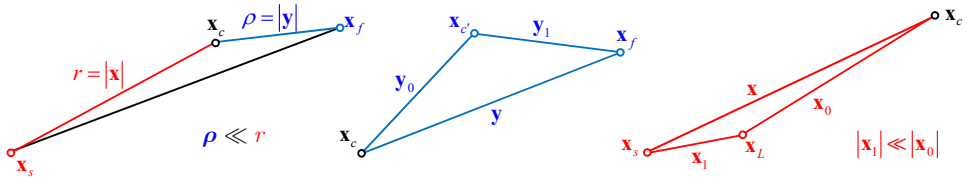

Figure 1: Basic scheme of an expansion about a pole $\mathbf{x}_c$ and schemes for further expansions about a field pole $\mathbf{x}'_c$ and a source pole $\mathbf{x}_L$.

up to a given level N of expansion and truncation order $O\left((\rho/r)^{N+1}\right)$. This may be immediately inferred from the one-dimensional expansion, for instance: $1/(x_f - x_s) \approx \sum_{n=0}^{N} (x_c - x_f)^n/(x_c - x_s)^{n+1} + O\left(((x_c - x_f)/(x_c - x_s))^{N+1}\right)$. In the above equation,

$$S_{n,m}(\mathbf{x}) = \frac{(n-m)!P_n^m(\cos\theta)e^{im\,\phi}}{r^{n+1}}, \quad R_{n,m}(\mathbf{y}) = \frac{P_n^m(\cos\beta)e^{im\,\alpha}}{(n+m)!}\rho^n$$
$$P_n^m(x) = \frac{(1-x^2)^{m/2}}{2^n n!}\frac{d^{n+m}}{dx^{n+m}}(x^2-1)^n, \tag{2}$$

where $P_n^m(x)$ are associated Legendre functions (polynomials). Both $S_{n,m}(\mathbf{x})$ and $R_{n,m}(\mathbf{x})$ are spherical harmonic functions. As reported by Gumerov and Duraiswami [2], the function name "S" above stands for *source* or *sender* and, coincidentally, also for *singular* (as $r \to 0$), whereas "R" means *receiver* as well as *regular*, which is much appropriate. According to the notation in eqn (1), each level $n = 0, 1, \ldots, N$ comprises $2n + 1$ terms. However, $S_{n,-m}(\mathbf{x}) = (-1)^m \bar{S}_{n,m}(\mathbf{x})$ and $R_{n,-m}(\mathbf{y}) = (-1)^m \bar{R}_{n,m}(\mathbf{y})$, $m = 1 \ldots n$, so that eqn (1) is actually implemented more compactly. The expressions of $S_{n,m}(\mathbf{x})$ and $R_{n,m}(\mathbf{x})$ are transformed to Cartesian coordinates in principle by solving for (r, θ, ϕ) and (ρ, β, α) in

$$\begin{array}{rrrl} \mathbf{x} = & \mathbf{x}_s - \mathbf{x}_c \equiv & (x_1, x_2, x_3) = & < r\cos\phi\sin\theta, r\sin\phi\sin\theta, r\cos\theta > \\ \mathbf{y} = & \mathbf{x}_f - \mathbf{x}_c \equiv & (y_1, y_2, y_3) = & < \rho\cos\alpha\sin\beta, \rho\sin\alpha\sin\beta, \rho\cos\beta > . \end{array} \tag{3}$$

Moreover, using the complex notation $x = x_1 + x_2 i$, $y = y_1 + y_2 i$ we are able to express $\bar{S}_{n,m}(\mathbf{x})$ and $R_{n,m}(\mathbf{y})$ compactly in Cartesian coordinates, as illustrated for $r^{2n+1}\bar{S}_{n,m}(\mathbf{x})$ and $R_{n,m}(\mathbf{y})$ with $m = 0 \ldots n,\ n = 0 \ldots 4$:

$$\begin{array}{ccccc} 1 & . & . & . & . \\ x_3 & \bar{x} & . & . & . \\ -|x|^2 + 2x_3^2 & 3\bar{x}x_3 & 3\bar{x}^2 & . & . \\ -9|x|^2 x_3 + 6x_3^3 & -3\bar{x}(|x|^2 - 4x_3^2) & 15x_3\bar{x}^2 & 15\bar{x}^3 & . \\ 9|x|^4 - 72x_3^2|x|^2 + 24x_3^4 & -15\bar{x}x_3(3|x|^2 - 4x_3^2) & -15\bar{x}^2(|x|^2 - 6x_3^2) & 105x_3\bar{x}^3 & 105\bar{x}^4. \end{array} \tag{4}$$

$$\begin{array}{ccccc} 1 & . & . & . & . \\ y_3 & \frac{1}{2}y & . & . & . \\ -\frac{1}{4}|y|^2 + \frac{1}{2}y_3^2 & \frac{1}{2}yy_3 & \frac{1}{8}y^2 & . & . \\ -\frac{1}{4}|y|^2 y_3 + \frac{1}{6}y_3^3 & -\frac{1}{16}y(|y|^2 - 4y_3^2) & \frac{1}{8}y_3y^2 & \frac{1}{48}y^3 & . \\ \frac{1}{64}|y|^4 - \frac{1}{8}y_3^2|y|^2 + \frac{1}{24}y_3^4 & -\frac{1}{48}yy_3(3|y|^2 - 4y_3^2) & -\frac{1}{96}y^2(|y|^2 - 6y_3^2) & \frac{1}{48}y_3y^3 & \frac{1}{384}y^4. \end{array} \tag{5}$$

These expressions can be pre-evaluated for a large number N of expansion levels using a symbolic software, such as Maple 15 (Maplesoft, a division of Waterloo Maple Inc., Waterloo, Ontario) – and some ingenuity – and stored in arrays (it is possible to apply a recursive scheme that directly works with the numerical values of $\mathbf{x}$ and $\mathbf{y}$ [1], [8]). In spite of the complex-variable notation, the indicated sum for every value of n in eqn (1) becomes real. In fact, it has been checked that each expansion level $n = 0 \ldots N$ in eqn (1) corresponds exactly to level $n+1$ of the multivariate Taylor series expansion of $1/4\pi|\mathbf{x}_f - \mathbf{x}_s|$ about $\mathbf{x}_c$, resulting in the truncation error $O\left((\rho/r)^{N+1}\right)$, as indicated. We must only pay attention to the orientation of the vector $\mathbf{x}_c - \mathbf{x}_s$, as shown in the left scheme of Fig. 1, which is just a notation subtlety introduced in the technical literature on the subject.

3 EXPRESSION OF THE NORMAL GRADIENT TO THE BOUNDARY

Since $\partial u^*/\partial \mathbf{y}_f \equiv \partial u^*/\partial \mathbf{y} = -\partial u^*/\partial \mathbf{x} \equiv \partial u^*/\partial \mathbf{x}_s$, the normal gradient to the boundary may be expressed in terms of derivatives of either $R_{n,m}(\mathbf{y})$ [1]–[3] or $S_{n,m}(\mathbf{x})$, the latter a more consistent proposition and slightly more accurate for less effort, as assessed next.

3.1 Expansion using derivatives with respect to the field point, according to the literature

An improved, compact complex notation of an otherwise classical approach starts with

$$\frac{\partial R_{n,m}(\mathbf{y})}{\partial y_1} + i\frac{\partial R_{n,m}(\mathbf{y})}{\partial y_2} = \begin{cases} -R_{n-1,m+1}(\mathbf{y}) & \text{if} \quad -n \le m \le n-2 \\ 0 & \text{otherwise} \end{cases}$$
$$\frac{\partial R_{n,m}(\mathbf{y})}{\partial y_3} = \begin{cases} R_{n-1,m}(\mathbf{y}) & \text{if} \quad -n+1 \le m \le n-1 \\ 0 & \text{otherwise} \end{cases} . \tag{6}$$

Then, making use of the notation $\vec{n} =< n_x,\ n_y,\ n_z >$ as well as of $n = n_x + i n_y \Rightarrow \bar{n} = n_x - i n_y$ for the components of the normal vector to the boundary, the normal gradient of the potential field turns out after some manipulation [13] – and taking into account the indicated constraints above – to be expressed as (numerical assessment in the next section)

$$q^* = -q_x^* n_x - q_y^* n_y - q_z^* n_z = k\frac{\partial u^*(\mathbf{x}_f - \mathbf{x}_s)}{\partial n} \equiv k\left[\frac{\partial u^*}{\partial x_f}n_x + \frac{\partial u^*}{\partial y_f}n_y + \frac{\partial u^*}{\partial z_f}n_z\right]$$
$$\approx \frac{k}{4\pi}\Re\sum_{n=1}^{N}\left(\sum_{m=-n}^{n-2}\bar{S}_{n,m}(\mathbf{x})R_{n-1,m+1}(\mathbf{y})\,\bar{n} - \sum_{m=-n+1}^{n-1}\bar{S}_{n,m}(\mathbf{x})R_{n-1,m}(\mathbf{y})\,n_z\right). \tag{7}$$

3.2 Novel proposition of derivatives expansion with respect to the source point

We propose to first pre-evaluate and store the expressions

$$\frac{\partial \bar{S}_{n,m}(\mathbf{x})}{\partial x_1} + i\frac{\partial \bar{S}_{n,m}(\mathbf{x})}{\partial x_2} = \bar{S}_{n+1,m-1}(\mathbf{x}), \qquad \frac{\partial \bar{S}_{n,m}(\mathbf{x})}{\partial x_3} = -\bar{S}_{n+1,m}(\mathbf{x}), \tag{8}$$

so that just one level more of terms $S_{n+1,m-1}(\mathbf{x})$ needs to be evaluated. Then, the normal gradient of the potential field to the boundary turns out to be expressed as simply as [13]

$$q^* = -q_x^* n_x - q_y^* n_y - q_z^* n_z = k\frac{\partial u^*(\mathbf{x}_f - \mathbf{x}_s)}{\partial n} \equiv -k\left[\frac{\partial u^*}{\partial x_s}n_x + \frac{\partial u^*}{\partial y_s}n_y + \frac{\partial u^*}{\partial z_s}n_z\right]$$
$$\approx \frac{k}{4\pi}\Re\left[\sum_{n=0}^{N}\sum_{m=-n}^{n}\left(-\bar{S}_{n+1,m-1}(\mathbf{x})\bar{n} + \bar{S}_{n+1,m}(\mathbf{x})n_z\right)R_{n,m}(\mathbf{y})\right]. \tag{9}$$

3.3 Conceptual and numerical assessments

Eqns (7) and (9) make use of complex variables just for the sake of simplicity as well as of code implementation, since all results should be real. The latter expression is not provided in the technical literature, although it is conceptually more consistent and simpler to implement. The advantage of using eqn (9) – as compared with eqn (7) – becomes evident also when it comes to the recursive application given by eqn (12), next section, as we just keep the index sequencing of $R_{n,m}(\mathbf{y})$.

The developments in eqn (9), obtained from

$$\frac{\partial u^*(\mathbf{x}_f-\mathbf{x}_s)}{\partial \mathbf{x}_f}=-\frac{\partial u^*(\mathbf{x}_f-\mathbf{x}_s)}{\partial \mathbf{x}_s}=\frac{k}{4\pi}\sum_{n=0}^{N}\sum_{m=-n}^{n}\frac{\partial \bar{S}_{n,m}(\mathbf{x})}{\partial \mathbf{x}}R_{n,m}(\mathbf{y})+O\big((\rho/r)^{N+1}\big)\,, \tag{10}$$

correspond to expanding the gradient of $u^*(\mathbf{x}_f-\mathbf{x}_s)$ in terms of multivariate Taylor series about $\mathbf{x}_s$ and the indicated truncation order, as checked symbolically with the Maple code.

On the other hand, the technical literature shows the results that lead to eqn (7) as

$$\frac{\partial u^*(\mathbf{x}_f-\mathbf{x}_s)}{\partial \mathbf{x}_f}=\frac{k}{4\pi}\sum_{n=0}^{N}\sum_{m=-n}^{n}\bar{S}_{n,m}(\mathbf{x})\frac{\partial R_{n,m}(\mathbf{y})}{\partial \mathbf{y}}+O\big((\rho/r)^{N}\big)\,, \tag{11}$$

although in general omitting that we are dealing with a truncation: N is just replaced with the less informative ∞. The latter is one order less accurate and more computationally intensive.

The accuracy of eqns (10) and (11) is assessed by means of two examples, both for $\mathbf{x}_f =< -11,\ 30.1,\ -30.1 >$ and $\mathbf{x}_s=\mathbf{0}$, but different expansion poles, $\mathbf{x}_c =< -11,\ 30,\ -30.1 >$ and $\mathbf{x}_c =< -11,\ 40,\ -30.1 >$, which leads to the ratios $\rho/r\approx 0.02317$ and $\rho/r\approx 0.19515$. Derivatives $\partial u^*(\mathbf{x}_f-\mathbf{x}_s)/\partial \mathbf{x}_f$ in the Cartesian coordinates are obtained according to eqns (10) and (11), for $N=0\ldots 11$ expansion levels, and Frobenius error norms of the expansions are plotted as shown on the left in Fig. 2. The solid, black lines are the expected error orders $O\left((\rho/r)^{N+1}\right)$ of a multivariate Taylor series expansion. The longdash, blue lines correspond to eqn (10), and the dashdot, red lines follow from eqn (11). The better accuracy obtained with eqn (10) (longdash, blue) coincides with just shifting horizontally to the left the results for eqn (11) (dashdot, red), according to the truncation errors indicated in those equations.

4 EXPANSION OF $R_{n,m}(\mathbf{x}_f-\mathbf{x}_c)$ ABOUT A NEW FIELD POLE $\mathbf{x}_{c'}$

The expansion of $R_{n,m}(\mathbf{x}_f-\mathbf{x}_c)$ in any of eqns (1), (7), (9) for $\mathbf{x}_f$ about a new pole $\mathbf{x}_{c'}$ may be expressed exactly, since $R_{n,m}(\mathbf{x}_f-\mathbf{x}_c)$ are polynomial terms, as

$$\underbrace{R_{n,m}(\mathbf{y})}\equiv\sum_{n'=0}^{n}\sum_{m'=-n'}^{n'}R_{n-n',m-m'}(\mathbf{y}_0)\underbrace{R_{n',m'}(\mathbf{y}_1)}, \quad |m-m'|\le|n-n'|\,, \tag{12}$$

where $\mathbf{y}\equiv\mathbf{x}_f-\mathbf{x}_c=(\mathbf{x}_f-\mathbf{x}_{c'})+(\mathbf{x}_{c'}-\mathbf{x}_c)=\mathbf{y}_1+\mathbf{y}_0$ (see the middle drawing of Fig. 1). Observe that, for successive expansions of the marked term, we characterize a level zero of expansion and follow from there on – expanding $\underbrace{R_{n',m'}(\mathbf{y}_1)}$ for $\mathbf{y}_1\equiv\mathbf{x}_f-\mathbf{x}_{c'}=(\mathbf{x}_f-\mathbf{x}_{c''})+(\mathbf{x}_{c''}-\mathbf{x}_{c'})\equiv\mathbf{y}_1+\mathbf{y}_0$ as the arguments of a recursive function – until arriving at the highest level. The clause $|m-m'|\le|n-n'|$ assures the existence condition of $R_{n-n',m-m'}(\mathbf{y}_1)$, which is void otherwise. We have checked that this expression is equivalent to the exact, multivariate Taylor series expansion of the polynomial terms

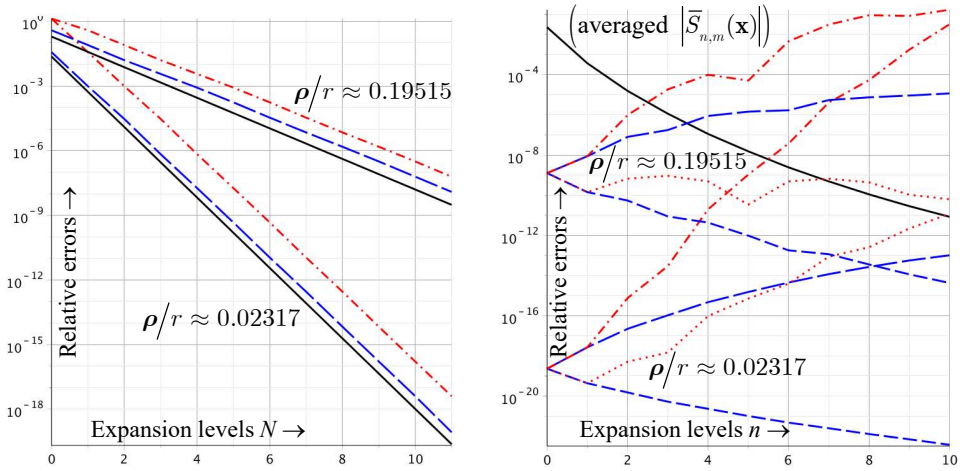

Figure 2: Left: relative errors of eqns (10) and (11) (longdash and dashdot lines), using $(\rho/r)^{N+1}$ (solid) as reference, for $N = 0 \ldots 10$; right: error assessments of eqn (13) (dashdot and dot) referred to averaged values of $\left|\bar{S}_{n,m}(\mathbf{x})\right|$, $n = 0 \ldots 10$ (solid), and compared with multivariate Taylor series (longdash and dash).

$R_{n,m}(\mathbf{x}_f - \mathbf{x}_c)$ about $\mathbf{x}_{c'}$. The above equation is not only consistent but also elegant, as the structure of $\underleftrightarrow{R_{n,m}(\mathbf{y})}$ is preserved when recursively passed as a function argument. It is given by Yoshida [1], eqn (B.11), and Liu [3], eqn (3.55), embeded in an "M2M (moment-to-moment) translation", and by Gumerov and Duraiswami [2], eqn (5.1.67), in the frame of a "local-to-local" translation – no authors seem to make reference to the indicated existence condition. This equation is to be applied recursively until we arrive at the highest level of the hierarchical pole development, when we proceed with the required boundary integrations.

5 EXPANSION OF $\bar{S}_{n,m}(\mathbf{x}_s - \mathbf{x}_c)$ ABOUT A NEW SOURCE POLE $\mathbf{x}_L$

The expansion of $\bar{S}_{n,m}(\mathbf{x}_s - \mathbf{x}_c)$ in any of eqns (1), (7), (9) for $\mathbf{x}_s$ about a new pole $\mathbf{x}_L$ is

$$\bar{S}_{n,m}(\mathbf{x}) = \sum_{n'=0}^{N} (-1)^{n'} \sum_{m'=-n'}^{n'} \bar{S}_{n+n',m+m'}(\mathbf{x}_0) \underleftrightarrow{R_{n',m'}(\mathbf{x}_1)} + O\left(\left(|\mathbf{x}_1| \,/\, |\mathbf{x}_0| \right)^{min(N+1,N+2-n)} \right), \quad n + n' \le N + 1, \tag{13}$$

where $\mathbf{x} \equiv \mathbf{x}_s - \mathbf{x}_c = (\mathbf{x}_s - \mathbf{x}_L) + (\mathbf{x}_L - \mathbf{x}_c) = \mathbf{x}_1 + \mathbf{x}_0$ (right drawing in Fig. 1). The upper limit N in the indicated sum for n' and the validity condition $n + n' \le N + 1$ take into account the existence of pre-evaluated expressions for $\bar{S}_{n,m}(\mathbf{x}_s - \mathbf{x}_c)$ up to level $N + 1$, as already needed in the expansion of eqn (8). We obtain either using symbolic Maple or, better, checking numerically for random *source*, *pole* and *local* points that this expression is equivalent to a multivariate Taylor series expansion with the indicated truncation order $O\left(\left(|\mathbf{x}_1| \,/\, |\mathbf{x}_0| \right)^{min(N+1,N+2-n)} \right)$, thus with decreasing accuracy as n increases, for a fixed N. It is given as eqn (B.7) by Yoshida [1] and in eqn (3.57) by Liu [3] for an "M2L (moment-to-local) translation", and by Gumerov and Duraiswami [2], eqn (5.1.68), for a "multipole-to-local" translation – although no authors seem to make reference to either the validity condition $n + n' \le N + 1$ or the truncation error, as they always set ∞ as the upper limit

for n' and do not mention how the equation is implemented in practice. It is worth remarking that the expansion of $\bar{S}_{0,0}(\mathbf{x})$ is mathematically the same task proposed in eqn (1). If we have to carry out further translations of $\overleftrightarrow{R_{n',m'}(\mathbf{x}_1)}$ in eqn (13), eqn (12) is to be used and then no more approximations take place (no need to ever refer to an "L2L translation" [1], [3]).

The graph on the right in Fig. 2 gives as reference averaged values $\left|\bar{S}_{n,m}(\mathbf{x})\right| \equiv \sum_{m=-n}^{n} \left|\bar{S}_{n,m}(\mathbf{x})\right|/(2n+1), n = 0 \ldots 10$ plotted as a solid, black line for $\mathbf{x}_s =< -11,\ 30.1,\ -30.1 >$ and $\mathbf{x}_c =< 0,\ 0,\ 0 >$, and we check that the magnitude of $\bar{S}_{n,m}$ decreases with increasing n (although it is quite invariant with $m = 0 \ldots n$ for a fixed n). We then carry out two numerical assessments, for expansions about $\mathbf{x}_L =< -10,\ 30,\ -30 >$ and $\mathbf{x}_L =< -10,\ 40,\ -30 >$, in such a way that $|x_1|\,/\,|x_0|$ is either ≈ 0.02317 or ≈ 0.19515. The longdash, blue lines are the relative errors for multivariate Taylor series expansions with error $O\left((\rho/r)^{N+1}\right)$, whereas the dashdot, red lines are relative errors obtained from eqn (13). Although they increase with increasing n, such errors, when related to the largest, averaged values $\left|\bar{S}_{0,m}(\mathbf{x})\right|$, tend to be much smaller, as given by the dash, blue and dot, red lines for multivariate Taylor series and eqn (13), respectively [13].

6 SOME REMARKS ON OUR IMPLEMENTED FM SCHEME

We consider an important achievement to have shown that the source pole expansion of eqn (13) leads to errors related to an increasingly truncated multivariate Taylor series, which on the other hand affect terms that decrease in magnitude as n increases. Our 2D and 3D implementations do not require such source pole expansions, since they follow the scheme of Fig. 3, with as many field pole expansions as required, according to the recursive scheme described in Section 4, thus involving no approximations other than the initial ones of eqn (1) for the potential fundamental solution, or either eqn (7) or (9) for the corresponding gradients (the latter one preferred, as already discussed). Accordingly, the highly condensed data corresponding to boundary integrations and matrix-vector multiplications inherent to the FMM are directly delivered to the source points, as shown in the figure, without making use of the source pole expansions of eqn (13). In fact, such source pole expansions – while introducing approximations errors, as assessed above – do not contribute to decreasing the computational effort needed in delivering data to any single one of the possibly millions of vector elements that come out from the FM matrix-vector multiplication, as convincingly assessed by Novelino [14]. We acknowledge that this subject deserves deeper investigation but it is worth remarking that our developments are in the frame of the so-called *reverse* FM

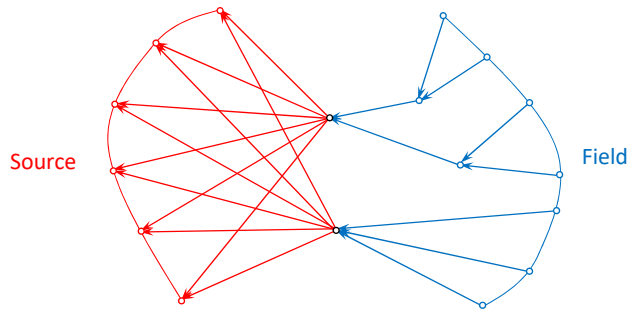

Figure 3: Proposed modified Middleman scheme with multilevel field pole expansions only.

scheme [4], for the outermost loop in terms of boundary elements, which may be, up to now only in the 2D case, curved and of arbitrarily high order.

7 TWO SIMPLE NUMERICAL ILLUSTRATIONS

7.1 Assessments for a convex domain

A convex domain in the shape of a tetrahedron as on the left in Fig. 4 is initially defined (Level $i = 0$) in terms of four faces ($F_0 = 4$ triangles) with vertex ($V_0 = 4$ node) coordinates

$$Coords = \begin{bmatrix} 1 & 2 & 3 & 4 \\ -3 & 3 & 0 & 0 \\ -1.5 & -1.5 & 1.5 & 0 \\ 0 & 0 & 0 & 4 \end{bmatrix}, \tag{14}$$

corresponding to $E_0 = V_0 + F_0 - 2 = 6$ (non-oriented) edges, according to Euler's theorem for a convex tetrahedron, with faces then successively subdivided into four triangles each, with the consequent creation of intermediate nodes, according to the scheme

$$\begin{aligned} &(F_0 = 4, \quad V_0 = 4, \quad E_0 = 6) \\ &F_i = 4F_{i-1}, \quad E_i = 2E_{i-1} + 3F_{i-1}, \quad V_i = E_i - F_i + 2, \quad i = 1, \ldots, 10. \end{aligned} \tag{15}$$

Increasingly refined meshes are considered for levels $2, \ldots, 10$, corresponding to $V_i =< 34, 130, 514, 2050, 8194, 32770, 131074, 524290, 2097154 >$ numbers of degrees of freedom (NDOFs), thus up to about two millions. Then, a succession of FMM analyses is carried out with the adjacency criterion Nc = 1, 2 or 3 (Nc is the number of levels of *children* elements that are considered adjacent to a given element, when source-element evaluations are carried out directly in the CBEM framework instead or resorting to FM expansions) and using N = 2, 4, 6, 8 or 10 Taylor expansion levels, according to eqn (1). The sketch on the left in Fig. 4 illustrates the case for a level 3 mesh ($V_3 = 130$), according to eqn (15). The

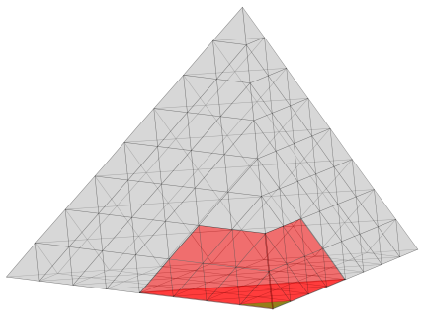

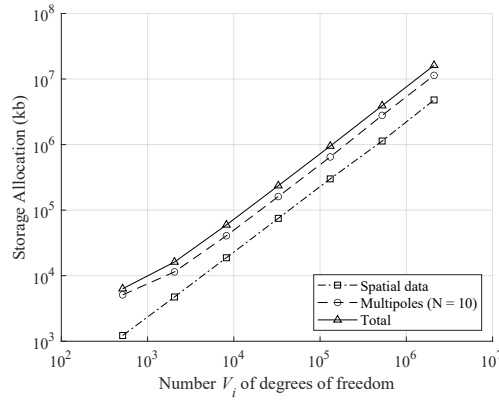

Figure 4: Red-colored elements, for $Nc = 2$, as the close ones to the green-colored element on the front bottom in a mesh corresponding to $V_3 = 130$ in eqn (15); and storage allocation for expansion level $N = 10$, $Nc = 3$ and different values of $V_i, i = 4, \ldots, 10$.

red-colored elements in this figure are the ones whose parents are adjacent to the parents of the green-colored triangle at the bottom face, thus for $Nc = 2$. The FM scheme is applied only for elements that are sufficiently far, that is, the gray-colored ones. The plot on the right in Fig. 4 shows the amount of storage allocated in the FMM evaluations for multipole expansions corresponding to $N = 10$, $Nc = 3$ and different values of $V_i, i = 4, \ldots, 10$. All evaluations are carried out in C++ running in Windows® 10 using a desktop computer CPU i7™-4770 with 3.4 GHz and 16 GB RAM.

Accuracy of the implemented FM scheme is firstly assessed for a linear potential field $u = x + y + z$ applied to the boundary of this tetrahedron, with nodal potentials $\mathbf{d}$ and gradient parameters $\mathbf{t}$ evaluated for $2, \ldots, 10$ mesh refinement levels, according to eqn (15). We carry out a control analysis in terms of the plain, but consistent conventional boundary element method (CBEM) [9], [10], [15], with all integrals evaluated analytically, for which the basic equation $\mathbf{Hd} = \mathbf{Gt}$ should be exactly satisfied within machine precision. Since the code is implemented in C++ with double precision, a relative error $\mathbf{e} = \|\mathbf{Hd} - \mathbf{Gt}\| / \|\mathbf{Hd}\| > 10^{-15}$ is expected to occur: actually increasing round-off errors take place as V_i (NDOF) increases. This is observed in the graph on the left in Fig. 5 for the error results marked as • related to refinement levels 2 through 6 in eqn (15). These errors are our achievable, threshold accuracy we can expect in the numerical simulations to come.

Observe that the implementations must start with refinement levels $Nc + 1$ in eqn (15). Since the T3 element exactly reproduces a linear potential field and all integrations are carried out within machine precision, the reported errors are due solely to the expansion truncations of the FM scheme, which are related to the truncation order at a given level N and ultimately depend on Nc. Here too, round-off errors unavoidably occur with increasing NDOF, which is reflected by the slightly ascending curves. These results lead to the accuracy threshold of results achievable in an analysis for the considered domain submitted to a more complicated potential field. In fact, a similar series of analyses carried out for an applied quintic field $u = 15x^2y^2z - 5z^3(x^2 + y^2) + z^5$, with results displayed on the right in Fig. 5, shows that accuracy convergence follows the pattern of the CBEM implementation until the threshold of the left graph is achieved. For some of the analyses results would still improve if a more refined mesh had been considered for higher values of Nc and N.

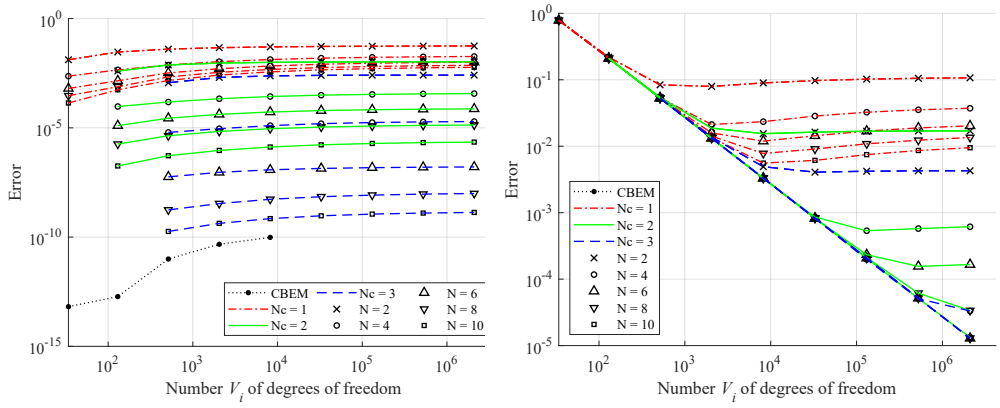

Figure 5: FMM relative error results for applied linear $u = x + y + z$ (left) and quintic $u = 15x^2y^2z - 5z^3(x^2 + y^2) + z^5$ potential fields for the example of Fig. 4.

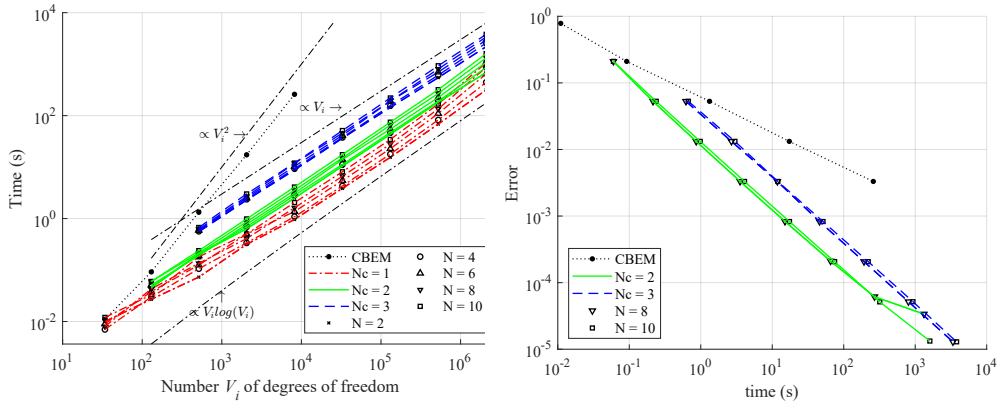

Figure 6: Computation times corresponding to the evaluations on the right in Fig. 5; and FMM performance assessment in terms of error vs. time for some analysis cases.

Fig. 6 shows on the left the computational time required for the matrix-vector multiplications **Hd** and **Gt** of the previous analyses. The computational times are proportional to V_i^2 and V_i for the CBEM and the FM operations, respectively, with time shifts perfectly acceptable for higher values of Nc and N, which attests to the advantage of working in such a computational framework even if just a few hundreds of degrees of freedom are required in a simulation. We are using here either analytical – thus time-consuming albeit exact – evaluations or the FMM scheme. Then, the indicated computational times can be lowered if adaptive numerical quadrature is implemented [8], [10], [15] for intermediary distances. The storage allocation is also relatively small and increases in proportion to the NDOF in a loglog plot, as already shown on the right in Fig. 4. The ultimate assessment of the proposed implementation is given in the graph on the right in Fig. 6, as we plot for the applied quintic potential field the relative errors of the right graph in Fig. 5 against the computational time on the left in Fig. 6 for a few values of Nc and N, also comparing with the CBEM. We see that not only the required computational time using the FMM is much smaller for a required error tolerance but also that the performance in terms of convergence rate is by far superior.

7.2 Assessments for a topologically challenging problem

Fig. 7 represents a very irregular 3D domain with a cavity, whose boundary is discretized with 16 linear triangle elements and 12 nodes. This is the FMM implementation of a numerical example presented in [9], [10], [15] to illustrate the use of machine precision evaluations for a topologically very challenging problem, which included the evaluation of potential and gradient results at internal points, a task not reproduced here.

The Cartesian coordinates of these nodes are, using the first row for the node numbering,

$$\left[\begin{array}{cccccccc:cccc} 1 & 2 & 3 & 4 & 5 & 6 & 7 & 8 & 9 & 10 & 11 & 12 \\ 1 & 1 & 0.2 & -1 & -2 & -1 & 0.5 & -0.25 & -0.3 & -0.5 & -0.4 & 0 \\ -0.5 & 0.4 & 0 & 0.5 & 0 & -0.5 & -1 & -0.55/3 & -0.2 & -0.1 & -0.3 & 0 \\ 0.5 & -0.5 & 1 & 1 & -0.2 & 0.5 & -1 & 0.05 & 0.3 & 0.4 & 0.5 & 0.6 \end{array}\right], \tag{16}$$

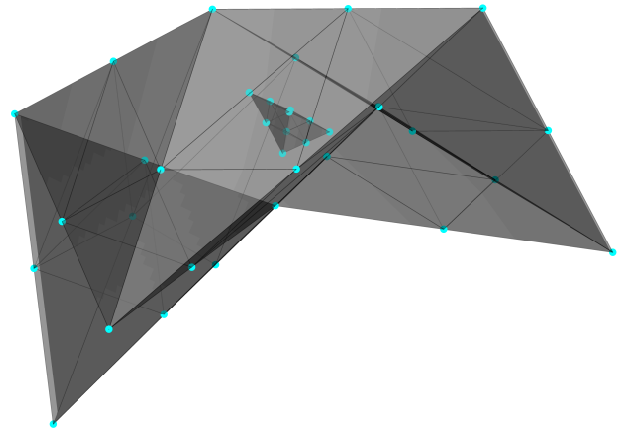

Figure 7: Very irregular domain with a cavity corresponding to the nodal and triangle incidence data of eqns (16) and (17).

and the nodal incidence is given, for the elements listed in the first row, by

$$\left[\begin{array}{cccccccccccc|cccc} 1 & 2 & 3 & 4 & 5 & 6 & 7 & 8 & 9 & 10 & 11 & 12 & 13 & 14 & 15 & 16 \\ 1 & 3 & 5 & 5 & 3 & 1 & 8 & 4 & 4 & 8 & 7 & 7 & 9 & 10 & 9 & 9 \\ 2 & 2 & 3 & 6 & 6 & 3 & 2 & 2 & 8 & 6 & 6 & 8 & 10 & 12 & 11 & 12 \\ 3 & 4 & 4 & 3 & 7 & 7 & 1 & 8 & 5 & 5 & 8 & 1 & 11 & 11 & 12 & 10 \end{array}\right]. \tag{17}$$

This corresponds to the level $i = 0$ discretization of a multiply connected domain made up of two disconnected boundaries, to which Euler's theorem applies in the modified form $E_0 = V_0 + F_0 - 4$. Nodes 9–12 in the level 0 refinement correspond to a cavity built up with elements 13-16. It is worth observing that elements 6 (nodes [1 3 7]) and 12 (nodes [7 8 1]) are almost coplanar. Successive mesh refinements are implemented according to the scheme

$$\begin{aligned} &(F_0 = 16, \quad V_0 = 12, \quad E_0 = 24) \\ &F_i = 4F_{i-1}, \quad E_i = 2E_{i-1} + 3F_{i-1}, \quad V_i = E_i - F_i + 4, \quad i = 1, \ldots, 10. \end{aligned} \tag{18}$$

Since this is a topologically very intricate problem, hierarchically distant elements in the mesh refinement are not necessarily distant geometrically, which demands an algorithm to check for actual distances within the topological structure, as developed by Santana [8] on the basis of Peixoto's [6] implementation for two-dimensional problems.

Increasingly refined meshes are considered for levels $2, \ldots, 8$, corresponding to NDOFs $V_i =< 132, 516, 2052, 8196, 32772, 131076, 524292 >$, thus up to half a million degrees of freedom. In a similar way as in the previous example, a succession of FMM analyses is carried out with the adjacency criterion Nc = 1, 2 or 3 and using N = 2, 4, 6, 8 or 10 multivariate Taylor expansion levels, according to eqn (1).

Accuracy of the implemented FMM scheme is firstly assessed for a linear potential field $u = x + y + z$ applied to the boundaries of the multiply connected body, with nodal potentials **d** and gradient parameters **t** evaluated for $V_i = 2, \ldots, 8$ mesh refinement levels, according to eqn (18). We also carry out a control analysis in terms of the plain, conventional

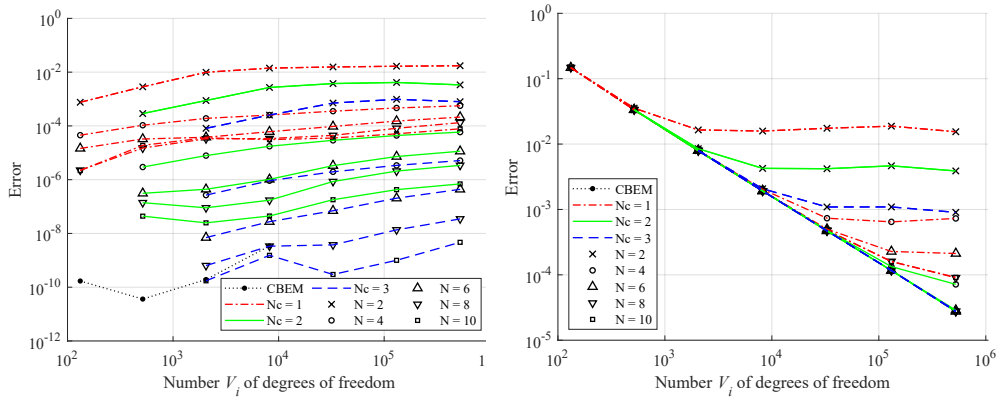

Figure 8: FMM relative error results for applied linear $u = x + y + z$ (left) and quadratic $u = x^2 + y^2 - 2z^2$ (right) potential fields to the domain of Fig. 7.

boundary element method (CBEM) with all integrals evaluated analytically [9], [10], [15], for which the basic equation $\mathbf{Hd} = \mathbf{Gt}$ should be exactly satisfied within machine precision. As in the previous example, a relative error $\mathbf{e} = \|\mathbf{Hd} - \mathbf{Gt}\| \,/\, \|\mathbf{Hd}\| > 10^{-15}$ is expected to occur and actually increasing round-off errors take place as the NDOF increases. The CBEM error results related to refinement levels 2 through 5 in eqn (18) are marked as • in the graph on the left in Fig. 8. These CBEM and FMM errors are our achievable, threshold accuracy we can expect in the numerical simulations to come.

Next, a series of analyses is carried out for an applied quadratic field $u = x^2 + y^2 - 2z^2$, with results displayed on the right in Fig. 8 showing that accuracy convergence follows the pattern of the CBEM implementation until the threshold of the left graph is achieved. In some cases results would still improve if a more refined mesh had been considered for higher values of Nc and N, as in the previous example. By the way, the assessments of Fig. 6 would be reproduced here almost unchanged, since for a very large mesh refinement the problem's topology no longer plays a remarkable role. Moreover, error results for higher-order potential fields would show the same pattern for very large NDOFs.

8 CONCLUDING REMARKS

It was our intention not to lay out the intricacy and manifoldness of the FMM. Readers are referred to Buchau [4], for instance, whose developments, more classical notation style and bibliographic references may be seen as complementary to and elucidative of many FMM features dealt with rather perfunctorily here.

This short communication focused on the conceptual aspects and the convergence issues of the series expansions needed in the 3D fast multipole developments for potential problems in a way that is not found in the technical literature. Important implementation details – particularly with respect to the recursive application of eqns (10) through (13) and the not lesser aspects of the iterative solution – GMRES, as implemented – of a practical problem had to be left to a posterior publication: both items are part of [8]. Two very simple examples, for which all integrals have been evaluated within machine precision, make evident how important it is to have evaluation precision, computational effort and accuracy of results completely under control. Owing to space restrictions we are not considering the application of adaptive numerical integration [8], [15] in which would be the typical course of action:

analytical integration [9], [10], [15] when source point and element are very close (relative distance to element about less than 1 [15]), numerical integration (Dunavant's scheme [8], [11], [15]) when source point and element are not too close but also not too far (decision to be made in terms of Nc) and, otherwise, FM scheme. With such adaptive layout the computational times showed in the graphs above would reduce drastically [8]. Our aim was just to address some relevant conceptual FMM issues, which could be dealt with adequately and isolated from numerical integration aspects and iterative solving schemes.

ACKNOWLEDGEMENT

This project was supported by the Brazilian agencies CAPES and CNPq.

REFERENCES

[1] Yoshida, K., Applications of fast multipole method to boundary integral equation method. PhD thesis, Department of Global Environmental Engineering, Kyoto University, 2001.
[2] Gumerov, N.A. & Duraiswami, R., *Fast Multipole Methods for the Helmholtz Equation in Three Dimensions*, Elsevier: Oxford, 2004.
[3] Liu, Y., *Fast Multipole Boundary Element Method: Theory and Applications in Engineering*, Cambridge University Press: New York, 2009.
[4] Buchau, A., Accuracy analysis of the fast multipole method for three-dimensional boundary value problems based on Laplace's equation. *WIT Transactions on Engineering Sciences*, vol. 131, WIT Press: Southampton and Boston, pp. 3–15, 2021.
[5] Dumont, N.A. & Peixoto, H.F.C., A fast-multipole unified technique for the analysis of potential problems with the boundary element methods. *Proceedings of the Indian National Science Academy*, **82**(2), pp. 289–299, 2016.
[6] Peixoto, H.F.C., A fast multipole method for high order boundary elements. PhD thesis, Pontifícia Universidade Católica do Rio de Janeiro, 2018.
[7] Florez Ttito, A.R., Implementation of a fast multipole technique for the solution of three dimensional potential and elasticity problems. PhD thesis, Pontifícia Universidade Católica do Rio de Janeiro, 2020. (In Portuguese.)
[8] Santana, H.M.S., Implementation of a consistent fast multipole technique for the solution of threedimensional potential problems. Master's thesis, Pontifícia Universidade Católica do Rio de Janeiro, 2022. (In Portuguese.)
[9] Dumont, N.A. & Kurz, T.G., Analytical 3D boundary element implementation of flat triangle and quadrilateral elements for potential and linear elasticity problems. *Boundary Elements and other Mesh Reduction Methods XLII*, eds A.H.D. Cheng & A. Tadeu, WIT Press: Southampton, pp. 1–11, 2019.
[10] Kurz, T.G., Analytical evaluation of the integrals of flat boundary elements for three-dimensional potential and elasticity problems. PhD thesis, Pontifícia Universidade Católica do Rio de Janeiro, 2021. (In Portuguese.)
[11] Dunavant, D.A., High degree efficient symmetrical Gaussian quadrature rules for the triangle. *International Journal for Numerical Methods in Engineering*, **21**, pp. 1129–1148, 1985.
[12] Dumont, N.A. & Santana, H.M.S., Boundary element analysis of 3D linear potential problems combining fast multipole expansion and machine-precision numerical integration. *CILAMCE-PANACM 2021 ONLINE (XLII Ibero-Latin-American Congress on Computational Methods in Engineering and 3rd Pan American Congress on Computational Mechanics)*, ABMEC: Rio de Janeiro, Brazil, 7 pp., 2021.
[13] Dumont, N.A., Basics of the 3D fast multipole method, Working paper, 2021.

[14] Novelino, L.S., Application of fast multipole techniques in the boundary element methods. Master's thesis, Pontifícia Universidade Católica do Rio de Janeiro, 2015. (In Portuguese.)
[15] Dumont, N.A. & Kurz, T.G., Analytical evaluation of all terms required in 3D potential and elastostatics boundary element implementations using linear triangle elements. *CILAMCE-PANACM 2021 ONLINE (XLII Ibero-Latin-American Congress on Computational Methods in Engineering and 3rd Pan American Congress on Computational Mechanics)*, ABMEC: Rio de Janeiro, Brazil, 7 pp., 2021.